

Spectral Analysis of the Temporal Self-Imaging Phenomenon in Fiber Dispersive Lines

Laura Chantada, Carlos R. Fernández-Pousa, *Member, IEEE*, and Carlos Gómez-Reino

Abstract—A spectral analysis of the temporal Talbot or self-imaging effect based on the exact computation of the radio frequency spectrum of the intensity of pulse trains after propagation in media with arbitrary first-order (β_2) and second-order (β_3) dispersion is presented. This allows the investigation of the performance of fiber dispersive lines as Talbot devices, where second-order dispersion is considered as a degradation factor. Conditions for repetition-rate multiplication and pulse compression over trains composed of linearly chirped Gaussian pulses, describing the effect as a filter in the intensity domain, are analyzed. The Talbot filter acts as a multiple bandpass filter that selects intensity harmonics. The filter's rejection capability depends on the train's spectral width normalized by the repetition-rate frequency of the output. The intensity fluctuations and pulse distortions of the output train are described from the spectral point of view. The tolerances of the filter under length and timing variations are also considered, and conditions for optimal filter stability are derived.

Index Terms—Optical fiber dispersion, optical pulses, pulse propagation, radio frequency (RF) spectrum, temporal Talbot effect.

I. INTRODUCTION

THE GENERATION of high-repetition-rate optical pulse trains is important in optical communications, photonic analog-to-digital conversion, photonic signal processing, and ultrafast optics. Although the most common alternative for the production of ultrafast trains is the use of mode-locked lasers, the temporal self-imaging or Talbot effect [1], [2] is also a well-established all-optical passive tool for its generation using a dispersive line [3]–[8]. Being a linear phenomenon, it allows integration with other linear processing techniques, such as compression [9] or reshaping [10]. Its tunability has also been demonstrated by the use of tunable dispersive lines [11], [12] and by switching to soliton regime [13]. Talbot dispersive lines have also been used together with nonlinear phenomena [12], [14], [15] and temporal imaging systems [16].

The use of both optical fiber [3]–[7], [13]–[16] and linearly chirped fiber Bragg gratings [8]–[12] for the specific objective of producing Talbot dispersive lines in the 1550-nm

Manuscript received May 25, 2005; revised January 26, 2006. This work was supported by the Ministerio de Educación y Ciencia, Spain, under Project TIC2003-03041. The work of L. Chantada was supported by the Ministerio de Educación y Ciencia, Spain, through a Formación del Profesorado Universitario grant.

L. Chantada and C. Gómez-Reino are with the Group of GRIN Optics, Department of Applied Physics, University of Santiago de Compostela, Campus Sur, Santiago de Compostela E15782, Spain (e-mail: falaura@usc.es; facgrc@usc.es).

C. R. Fernández-Pousa is with the Signal Theory and Communications Division, Department of Physics and Computer Engineering, Universidad Miguel Hernández, Elche E03202, Spain (e-mail: c.pousa@umh.es).

Digital Object Identifier 10.1109/JLT.2006.872681

band has been reported. Several authors have paid attention to the performance of the effect in these media. When using linearly chirped Bragg gratings, dispersion deviation [2] and dispersion ripple [2], [17] are the main deleterious factors. In fiber dispersive lines, the corresponding limiting factors are the dispersion deviations induced by higher order dispersion, or the length or timing deviations.

Although the experimental analysis of the Talbot-imaged trains usually focuses on the time domain, much information can be inferred from a spectral analysis of the intensity of the train [5], [6]. In conventional filters designed to increase the repetition rate based on optical spectral filtering, a linear filter suppresses the optical harmonics of the input train that do not belong to the high-frequency output train (see, for instance, [12] for different architectures). Therefore, the performance of these systems can be analyzed from the optical transfer function of the linear filter. In contrast, and because dispersion is a phase-only filter in the optical domain, Talbot dispersive filtering is nonlinear and requires a spectral analysis in the intensity domain.

The first objective of this paper is to compute and analyze the intensity spectrum of coherent optical trains after a dispersive line with arbitrary first-order (β_2) and second-order (β_3) dispersion as a model of fiber-based Talbot devices. Then, we describe the Talbot fiber dispersive lines as filters in the radio frequency (RF) or intensity domain. The technique used in this paper permits an easy identification of the spectral traces of the interference terms arising in dispersive pulse propagation [18]–[23]. High-repetition-rate intensity trains can be obtained even in the presence of second-order dispersion by means of Talbot filtering if the input trains have the appropriate optical spectral content. The rejection capability of RF intensity harmonics and the tolerance under timing and line length variations will be discussed. In particular, a design rule that determines the optical spectral width that maximizes the tolerance of the Talbot filters is derived.

Throughout this paper, we consider the Talbot dispersive lines as defined by matching their accumulated first-order dispersion, whereas second-order dispersion is a deviation from the ideal behavior. Although several authors have studied Talbot dispersive lines defined by matching first-, second-, or even higher order dispersion [1], [7], [24], this point of view will not be pursued in this paper.

This paper is organized as follows: In Section II, we present the exact computation of the intensity spectrum of Gaussian pulse trains after a dispersive line with arbitrary first- and second-order dispersion. In Section III, we explore the different spectral intensity patterns associated with Talbot dispersive

lines by analyzing a number of examples. In Sections IV and V, we characterize the rejection capability of the Talbot dispersive filters as well as their tolerance under length and timing variations. Finally, Section VI presents our conclusion.

II. INTENSITY SPECTRUM IN DISPERSIVE LINES

The propagation of modulated signals carried by a monochromatic optical wave with frequency ω_0 through a linear dispersive medium with negligible attenuation is described by a slowly varying complex envelope $e(t, z)$. The equation governing its propagation is given by [25]

$$\frac{\partial e}{\partial z} + \frac{i}{2}\beta_2 \frac{\partial^2 e}{\partial t^2} + \frac{1}{6}\beta_3 \frac{\partial^3 e}{\partial t^3} = 0. \quad (1)$$

In this formula, z is the length along the direction of propagation, and t is the time measured in the propagating reference frame $t = t_{\text{phy}} - \beta_1 z$, where t_{phy} is the physical time, and β_1 , β_2 , and β_3 are the inverse of the group velocity and the first- and second-order dispersion coefficients, respectively. These are the coefficients of the expansion of the propagation constant $\beta(\omega_0 + \omega)$ around the optical carrier ω_0 . Higher order dispersion is considered negligible.

Let us assume that such a dispersive line is fed with a periodic train of linearly chirped Gaussian pulses expressed as

$$e(t, 0) = \sum_{k=-\infty}^{+\infty} \exp \left[-\frac{(t - kt_0)^2 (1 + iC)}{2t_p^2} \right] \quad (2)$$

where C is the linear chirp or phase-modulation parameter of the pulses, t_p is their width, which is measured as the half-width at $1/e$ decay in power, and t_0 is the period of the train. The repetition rate of the train will be described by its angular frequency $\Omega_0 = 2\pi/t_0$.

The propagation of the amplitude (2) in a dispersive medium of length L can be solved in Fourier domain $E(\omega, L) = H(\omega, L)E(\omega, 0)$. In this formula, the input field is given by

$$E(\omega, 0) = t_p \left[\frac{2\pi}{(1 + iC)} \right]^{\frac{1}{2}} \exp \left[-\frac{(1 - iC)\omega^2}{2\sigma_\omega^2} \right] \Omega_0 \sum_m \delta(\omega - \Omega_0 m) \quad (3)$$

where the sum ranges from $-\infty$ to ∞ , and $\sigma_\omega = (1 + C^2)^{1/2}/t_p$ is the optical spectral width of the individual pulses, which is measured as the half-width at $1/e$ decay in power. $H(\omega, L)$ is the transfer function of linear propagation defined as

$$H(\omega, L) = \exp \left(\frac{i\beta_2 L \omega^2}{2} + \frac{i\beta_3 L \omega^3}{6} \right). \quad (4)$$

Due to the structure of quadratic phases in (3) and (4), we define, for future use, the equivalent dispersion of the line as

$$D_{\text{eq}} = \left| \beta_2 L + \frac{C}{\sigma_\omega^2} \right|. \quad (5)$$

This is the relevant quantity when considering linear pulse compression in a dispersive line [25].

The detected signal after its propagation through the dispersive line $i(t, L) = |e(t, L)|^2$ is given in the spectral domain $I(\omega, L)$ by the autocorrelation of $E(\omega, L)$. The result is given by

$$I(\omega, L) = \Omega_0 \zeta(\omega)^{-\frac{1}{2}} J(\omega) f(\omega) \sum_k \delta(\omega - k\Omega_0) \quad (6)$$

where

$$\zeta(\omega) = 1 - \frac{i\beta_3 L \sigma_\omega^2 \omega}{2} \quad (7)$$

$$J(\omega) = t_p \sqrt{\pi} \exp \left(-\frac{\omega^2}{4\sigma_\omega^2} + \frac{i\omega^2 \text{Im}(\zeta(\omega))}{12\sigma_\omega^2} \right) \quad (8)$$

$$f(\omega) = \sum_n g_n(\omega) \exp \left(\frac{i\omega n t_0}{2} \right) \quad (9)$$

and

$$g_n(\omega) = \exp \left[-\frac{(\omega - \omega_n)^2 D_{\text{eq}}^2 \sigma_\omega^2}{4\zeta(\omega)} \right] \quad (10)$$

where $\omega_n = nt_0/D_{\text{eq}}$, and $\text{Im}(\zeta(\omega))$ is the imaginary part of $\zeta(\omega)$. From (6), the two-sided power spectrum density (PSD) of the train intensity can be computed as

$$S(\omega, L) = \Omega_0 |J(\omega) f(\omega)|^2 |\zeta(\omega)|^{-1} \sum_k \delta(\omega - k\Omega_0). \quad (11)$$

The power carried by each harmonic $k\Omega_0$ is determined by the smooth functions $J(\omega)$ and $\zeta(\omega)$ and the peaked function $f(\omega)$. The first function $J(\omega)$ is broadband, and its modulus is dispersion independent. Its bandwidth, which is measured as the half-width of 30-dB decay in power, is $3.72\sigma_\omega$. This function determines the highest significant frequency of the RF spectrum $\omega_{\text{max}} \cong 3.72\sigma_\omega$.

On the other hand, $\zeta(\omega)$ contains the only dependence on β_3 in the spectrum. Second-order dispersion is negligible, i.e., $\zeta(\omega) \cong 1$, when its value for the highest significant frequency is negligible. We will describe the relative influence of β_3 by the following angular parameter:

$$\varepsilon = 1.86\beta_3 L \sigma_\omega^3 \quad (12)$$

so that the negligible β_3 is equivalent to $\varepsilon \ll \pi$. Nonnegligible values of ε account for a narrowing of the total bandwidth of the spectrum through the factor $|\zeta(\omega)|^{-1}$.

Finally, the function $f(\omega)$ is essentially a sum of dispersion-dependent peaked functions $g_n(\omega)$, which is indexed by an integer number n . These functions are centered at $\omega_n = nt_0/D_{\text{eq}}$ and have a Gaussian functional form when β_3 is negligible. In this limit, the spectral width of all functions $g_n(\omega)$ is proportional to $1/\sigma_\omega D_{\text{eq}}$. Then, these functions are narrower as the spectral width of the pulses is larger. Furthermore, they get broader as the equivalent dispersion D_{eq} reduces and lie closer to each other as the dispersion increases. When β_3 is not negligible, the functional form of functions $g_n(\omega)$ becomes non-Gaussian. Their width is enlarged progressively along the

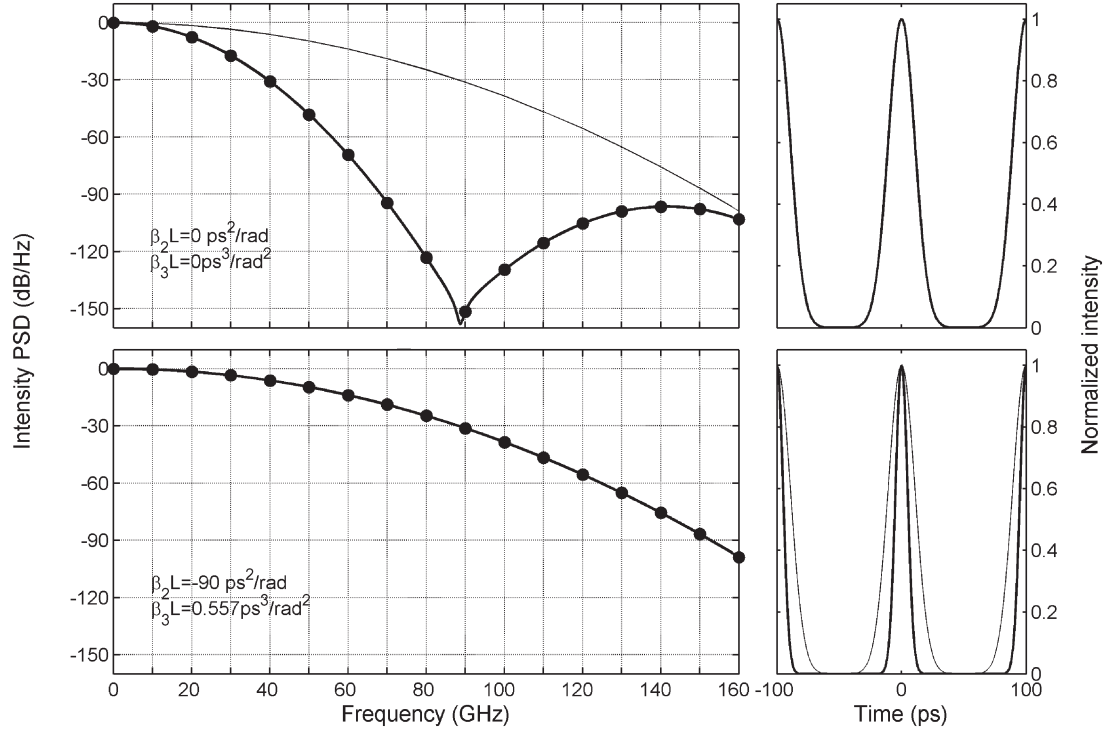


Fig. 1. Intensity PSD (left) and temporal intensity (right) of a 10-GHz train before (top) and after (bottom) its propagation in a standard SMF of length $L = 4.29$ km (compression length).

RF spectrum through the factor $\zeta(\omega)$ in (10), although their global behavior is similar.

The quantities $g_n(\omega)$, with $n \neq 0$, describe the spectral content of the interference pattern arising in the dispersion of a given pulse and its n th neighbor, whereas $g_0(\omega)$ is associated with the single-pulse spectrum. The properties of the ratio $g_1(\omega)/g_0(\omega)$, which account for intersymbol interference, have been described in [23].

We now illustrate spectrum (11) by means of a simple example describing linear pulse compression. In Fig. 1, we show the intensity PSD and the detected temporal signal of a 10-GHz train after its propagation through a standard single-mode fiber (SMF) carried by a monochromatic wave at $\lambda = 1550$ nm ($\beta_2 = -21$ ps²/km · rad and $\beta_3 = 0.13$ ps³/km · rad²). The trains are composed of Gaussian pulses with chirp $C = 2$ rad and $t_p = 15$ ps, so that the significant portion of the spectrum extends from dc to 88 GHz. On the left-hand side of both figures, we present the positive-frequency portion of the two-sided intensity PSD (11), and on the right-hand side, we present the corresponding intensity profiles. The broadband spectral envelope $|J(\omega)|^2/|\zeta(\omega)|$ is depicted with a thin continuous curve. The thick continuous curve represents the product $|J(\omega) \cdot f(\omega)|^2/|\zeta(\omega)|$ that controls the power carried by each harmonic of the output intensity train. The power of the harmonics is the value of this thick line at the multiples of the fundamental frequency $\Omega_0 = 2\pi \times 10$ GHz, which are depicted with dots. On the right-hand side, the thin continuous curve represents two periods of the intensity of the input train, and the thick curve represents two periods of the output intensity. The intensity PSD has been normalized to 0 dB at the carrier, whereas the temporal signals have been normalized to unity at

the center of the period to help visualize the pulse interference patterns.

In Fig. 1, the trains are propagated through an SMF with two lengths, i.e., $L = 0$ (initial train, top) and $L = 4.29$ km (bottom). β_3 is negligible in both examples ($\varepsilon = 0$ and $\varepsilon = 0.0034$ rad, respectively). The intensity PSD of the input train (top) has two lobes that group the harmonics of the intensity. They are centered at dc and 140 GHz and are associated with the first two contributions to the sum $f(\omega)$ in (11). Because their spectral overlapping is negligible, the sum can be approximated to $|g_0(\omega)|^2 + |g_1(\omega)|^2$. The first lobe $|g_0(\omega)|^2$, together with the overall envelope, represents the intensity spectrum of a single pulse. The second lobe $|g_1(\omega)|^2$, which is centered at 140 GHz, is due to the slight interference between the neighboring Gaussian pulses. In practice, no pulse-to-pulse interference is present in the input train, so that the intensity harmonics should be grouped in a single lobe centered at dc. Additional interference lobes only appear as dispersion causes pulse broadening and subsequent interference [26].

The existence of interference lobes is a limitation of the representation of the input train as a coherent sum of Gaussian pulses, i.e., their infinite temporal extension causes pulse-to-pulse overlapping and interference even in the input signal. However, the value of the power of the harmonics describing the neighboring-pulse interference term, which is more than 90 dB below the carrier, is sufficiently small to rely on the validity of the model.

The second example in Fig. 1 (bottom) shows the signal after the compression length, where pulses reach the minimum temporal width $1/\sigma_\omega = 6.7$ ps. At this length, the equivalent dispersion D_{eq} defined in (6) vanishes. This means that

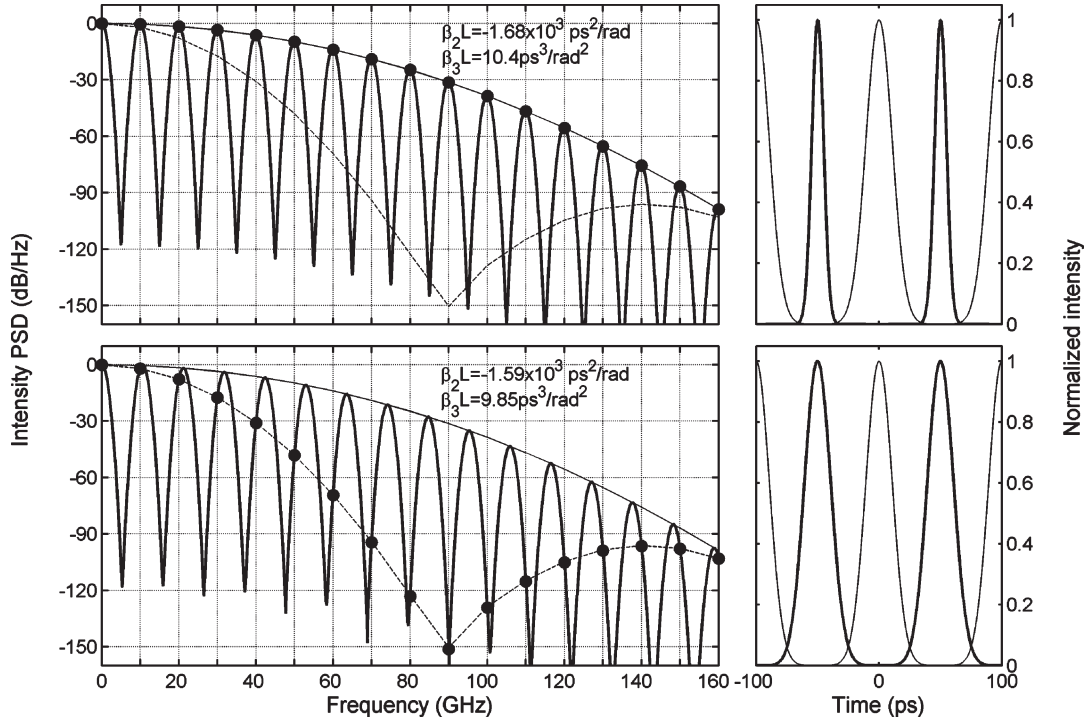


Fig. 2. Intensity PSD (left) and temporal intensity (right) of a 10-GHz train after its propagation in SMF of length $L = 80.1$ km (top) and 75.8 km (bottom), which correspond to the compressing Talbot and standard Talbot conditions with index $\gamma/\alpha = 1$, respectively.

$|f(\omega)|^2 \cong |g_0(\omega)|^2 = 1$ [see (10) and the definition of ω_n] so that the spectrum follows the envelope $|J(\omega)|^2/|\zeta(\omega)|$. In other words, this is the single-pulse envelope of compressed pulses.

III. INTENSITY SPECTRUM IN THE TEMPORAL SELF-IMAGING PHENOMENON

The temporal Talbot or self-imaging phenomenon is the formation of intensity trains by multiple pulse interference in a first-order dispersive system. It arises when the accumulated first-order dispersion is of the following form:

$$|\beta_2 L| \Omega_0^2 = \frac{2\pi\gamma}{\alpha} \quad (13)$$

where α and γ are positive and coprime integers, and the repetition-rate frequency is Ω_0 . The output is a replica of the original train when the product $\alpha\gamma$ is even and a replica of the original train, which is shifted by half a period $t_0/2$, when $\alpha\gamma$ is odd. In general, the output train has a repetition rate $\alpha\Omega_0$. The case $\alpha = 1$ is called the integer Talbot effect, and the output has no increase in the rate. When α differs from unity, the effect is called fractional Talbot [2].

Due to the structure of the quadratic phases in (2)–(4), another value of total dispersion, which is expressed by the following equation, is of interest:

$$D_{\text{eq}} \Omega_0^2 = \left| \beta_2 L + \frac{C}{\sigma_\omega^2} \right| \Omega_0^2 = \frac{2\pi\gamma}{\alpha}. \quad (14)$$

We will refer to (14) as the compressing Talbot condition. To interpret this condition, let us first consider that the length of the dispersive medium is adjusted to verify (14). The output

signal is a Talbot image (integer or fractional, depending on α) of a train of compressed pulses. Let us further suppose that phase modulation and dispersion have opposite signs, i.e., $C \cdot \beta_2 < 0$, so that the length of the medium can be split in two positive contributions, i.e., $L = L_C + L_T$, the first being the compression length. The first part of the line is used to compress the pulses in the train individually, and the remaining length of the fiber L_T produces the Talbot image of the train of compressed pulses. If both phase modulation and dispersion have the same sign, i.e., $C \cdot \beta_2 > 0$, the compression condition (14) produces the same overall result, because the final structure of the spectral phases is equal to the previous case, i.e., $C \cdot \beta_2 < 0$. Between the Talbot and the compressing Talbot conditions (13) and (14), a continuum of partial compression is obtained.

We analyze now the intensity spectrum of the temporal Talbot effect by means of some representative examples. Let us first consider an integer self-imaging dispersive line with index $\gamma/\alpha = 1$ (Fig. 2). Pulses have a width of 15 ps and a chirp $C = 2$ rad, as in Fig. 1. The dispersive medium is an SMF at $\lambda = 1550$ nm, and compressing conditions are shown in the figures at the top, whereas noncompressing conditions are depicted at the bottom. In both examples, second-order dispersion is negligible ($\varepsilon = 0.064$ and 0.061 , respectively).

From Fig. 2, we can interpret how Talbot effect creates the self-images of the train. Multiple pulse-to-pulse interference is reflected in the structure of dips and bumps of the function $|J(\omega) \cdot f(\omega)|^2/|\zeta(\omega)|$. This structure is due to the sum over $g_n(\omega)$ in $f(\omega)$ [see (9)]. In the absence of second-order dispersion, the spectral separation between consecutive functions $g_n(\omega)$ and $g_{n+1}(\omega)$ is t_0/D_{eq} , whereas their spectral width goes as $1/\sigma_\omega D_{\text{eq}}$. Then, for the fiber lengths of the order of magnitude of the Talbot distances, so that $D_{\text{eq}} \sim 1/\Omega_0^2$,

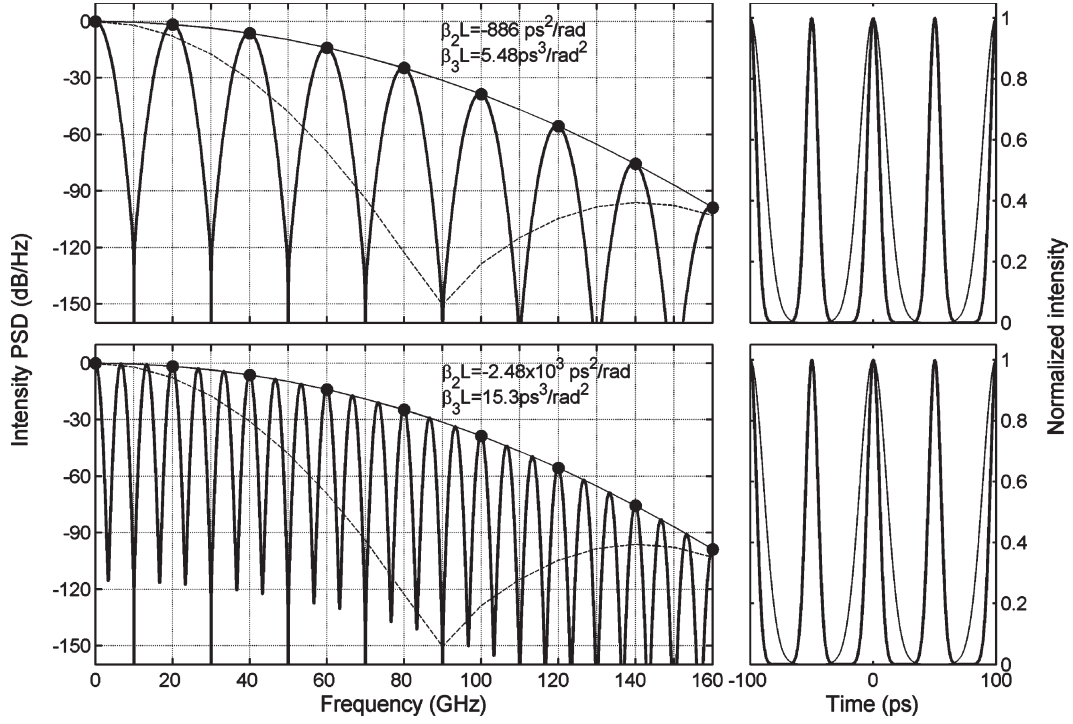


Fig. 3. Intensity PSD (left) and temporal intensity (right) of a 10-GHz train after its propagation in a standard SMF of length $L = 42.2$ km (top) and 118 km (bottom), which correspond to the compressing Talbot condition with indexes $\gamma/\alpha = 1/2$ and $3/2$, respectively.

the spectral overlapping between functions $g_n(\omega)$ can be neglected if $\sigma_\omega \gg \Omega_0$. Then, $|f(\omega)|^2$ can be approximated by $\sum_n |g_n(\omega)|^2$, and the intensity PSD can be rewritten as

$$S(\omega, L) \cong \Omega_0 |J(\omega)|^2 |\zeta(\omega)|^{-1} \sum_s G_s(\omega) \sum_k \delta(\omega - k\Omega_0) \quad (15)$$

where $G_n(\omega) = |g_n(\omega)|^2$. Dispersion thus acts as a multiple bandpass filter, in which the positions and width of the passbands are determined by $G_n(\omega)$. Their centers are located at $\omega_n = n t_0 / D_{\text{eq}}$, and their 30-dB decay half-width, if second-order dispersion is negligible, is obtained by

$$\Delta\omega = \frac{3.72}{\sigma_\omega D_{\text{eq}}}. \quad (16)$$

Then, in Fig. 2 (top), it can be observed that the output harmonics of the compressing Talbot replica of the original train lie at the center of the n th passband that describes the interference between pulses separated by n time slots. In other words, the n th harmonic of the intensity train is created by the interference of pulses separated by n time slots. Under noncompressing Talbot condition, the behavior of the intensity PSD is similar, but the output harmonics do not lie on the passband's centers (see Fig. 2, bottom).

This point of view can be further explored by considering the examples presented in Fig. 3. The same train is propagated through an SMF up to the compressing Talbot lengths with indexes $1/2$ and $3/2$. Again, second-order dispersion is negligible ($\varepsilon = 0.034$ and 0.094 , respectively). The output train is similar, because in both examples, the output is a 20-GHz train of transform-limited pulses. However, the interference structures are different. In the first example (top), the h th output harmonic

is created by the interference of pulses separated by h time slots, whereas in the second example (bottom), it is created by the interference of pulses originally separated by $3h$ time slots.

In general, the passbands associated with the compressing Talbot lines are centered at $\omega_n = n\alpha\Omega_0/\gamma$, in which n is the index determining the interference between pulses separated by n time slots. When n is a multiple of γ , i.e., $n = h\gamma$ for certain integer h , the passband is centered at the h th output harmonic $h\alpha\Omega_0$. Then, if the compressing Talbot line is an integer ($\alpha = 1$), the h th harmonic lies at the center of the passband with index $n = h\gamma$, so that all the harmonics survive and, between two consecutive harmonics, there are $\gamma - 1$ passbands. Conversely, if the compressing dispersive line is fractional ($\alpha \neq 1$), only the frequency multiples of the α th input harmonic lie at the center of a passband. These surviving harmonics create the spectral content of the output train, with the remaining harmonics being filtered.

The next example in Fig. 4 explores the suppression of harmonics in Talbot devices with index $1/3$ and its dependence on the optical linewidth. A 10-GHz train with 15-ps-wide pulses is launched into an SMF compressing dispersive line with index $1/3$. In the top part of the figure, the chirp parameter of the pulses is $C = 2$ rad, so that the width of the compressed pulses is 6.7 ps. In contrast, the chirp parameter of the pulses at the bottom part is $C = 1$ rad, and thus, the compressed pulses are 10.6 ps wide. Second-order dispersion is still negligible ($\varepsilon = 0.0237$ and 0.0062 , respectively). We observe that the suppression of harmonics that do not belong to the output 30-GHz train is not exact. These harmonics will be referred to as residual harmonics. The partial suppression of residual harmonics is due to the finite width of the bandpass $G_n(\omega)$, which are, according to (16), inversely proportional to the spectral width.

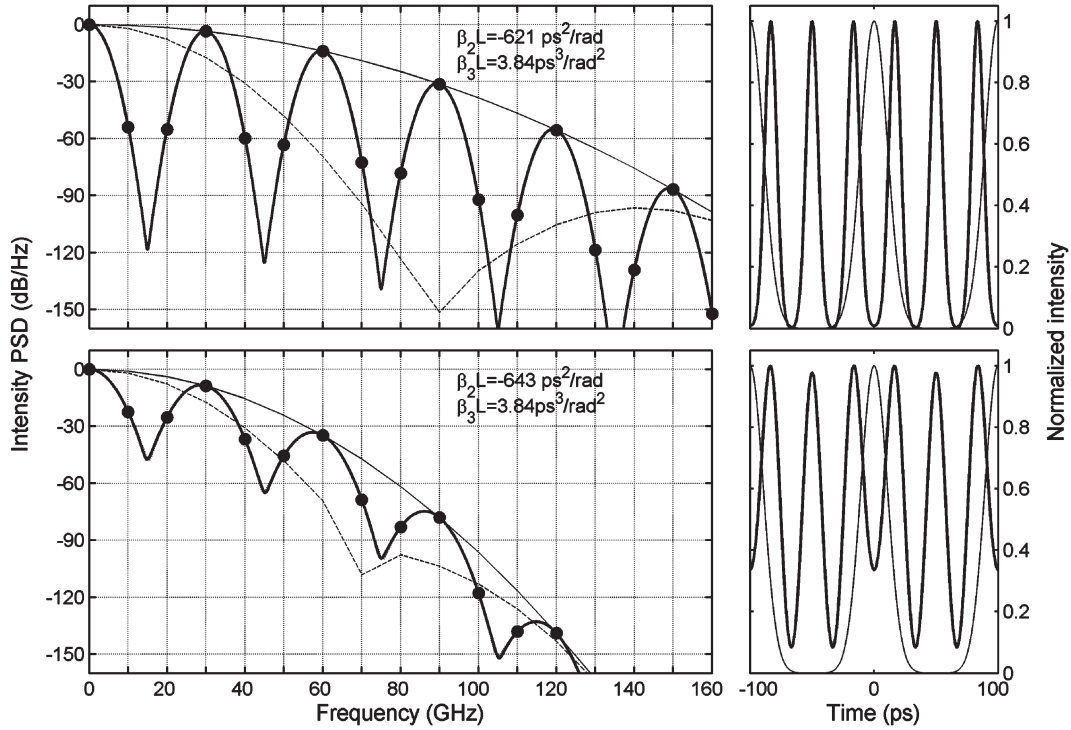


Fig. 4. Intensity PSD (left) and temporal intensity (right) of a 10-GHz train after its propagation in a standard SMF of length $L = 29.5$ km (top) and 30.6 km (bottom), which correspond to the compressing Talbot condition with index $1/3$. Pulses have a width of 15 ps and chirp $C = 2$ rad (top) and $C = 1$ rad (bottom).

In Fig. 4 (bottom), we observe that a reduction of the spectral width implies, from the temporal point of view, that pulses overlap in the output train causing pulse pedestal and intensity fluctuation. As a result, the temporal profile shows a periodic structure with frequency Ω_0 , reflecting the absence of exact repetition-rate multiplication. From the spectral point of view, we notice, on one hand, the reduction of the spectrum and, on the other, the increase of the power carried by residual harmonics due to the broadening of the passbands $G_n(\omega)$. The inefficient filtering of residual harmonics is clearly shown at 10 and 20 GHz.

Notice that only the semiinteger fractional Talbot lines with index $\gamma/\alpha = (2k + 1)/2$ produce a total suppression of residual harmonics [6]. This exact cancellation occurs if the input pulses are transform limited, i.e., if the input envelope is a real function so that its Fourier coefficients in (3) verify that $\varphi_m = -\varphi_{-m}$. This, together with the spectral phases caused by dispersion, produces a relative phase shift of $\pm\pi$ between optical spectral lines with indexes $\pm m$, which implies the total suppression of the residual harmonics. This observation is similar to the carrier suppression effect in analog communications [27].

To conclude this section, we consider the last example in Fig. 5, where second-order dispersion is not negligible. A 20-GHz train of pulses with a width of 5 ps and chirp $C = 2$ rad is propagated through a dispersion-shifted fiber (DSF; $\beta_2 = -0.5$ ps²/km · rad and $\beta_3 = 0.07$ ps³/km · rad² at $\lambda = 1550$ nm), whose length is adjusted to verify the compressing Talbot condition $\gamma/\alpha = 1/3$ (top) and $2/3$ (bottom). The thin continuous and dashed curves represent the envelope of the intensity PSD that would correspond to the compressing Talbot and noncompressing Talbot conditions, respectively, if the second-order dispersion coefficient was zero.

The top figure ($\varepsilon = 3.32$) shows a slight decrease of overall bandwidth, as compared with the $\beta_3 = 0$ case, and a progressive broadening of the passbands' widths, which can be approximated by

$$\Delta\omega \cong \frac{3.72 |\zeta(\omega_n)|^{1/2}}{\sigma_\omega D_{\text{eq}}}. \quad (17)$$

The width enlargement is due to the factor $|\zeta(\omega)|^{1/2}$ and weakens the suppression or filtering of residual harmonics. Therefore, the output signal contains high frequencies that are manifested in the time domain as the oscillatory structure in the pulse's trailing edge. For future use, the following equation computes the maximum value of the 30-dB passband half-width in the significant part of the spectrum, i.e., $\omega \sim 3.72\sigma_\omega$:

$$\Delta\omega_{\text{max}} \cong \frac{3.72(1 + \varepsilon^2)^{1/4}}{\sigma_\omega D_{\text{eq}}} \quad (18)$$

where (12) has been used. Notice that, despite the presence of a significant β_3 dispersion, the train in Fig. 5 (top) has no intensity fluctuations, broadening, or pedestal, the only impairment is the distortion induced by the second-order dispersion.

If the influence of β_3 is sufficiently large, the passbands overlap, causing the fading of the multiple passband structure. The approximation leading to (15) is no longer valid, and it is required to resort to (4) for the correct description of the intensity PSD. This is shown in Fig. 5 (bottom) where the β_3 influence is now larger ($\varepsilon = 6.41$). Notice that in this regime, the output signal shows periodic variations in pulse intensity in addition to pulse distortion. Pulse intensity fluctuations are periodic due to the underlying nonfiltered input harmonics.

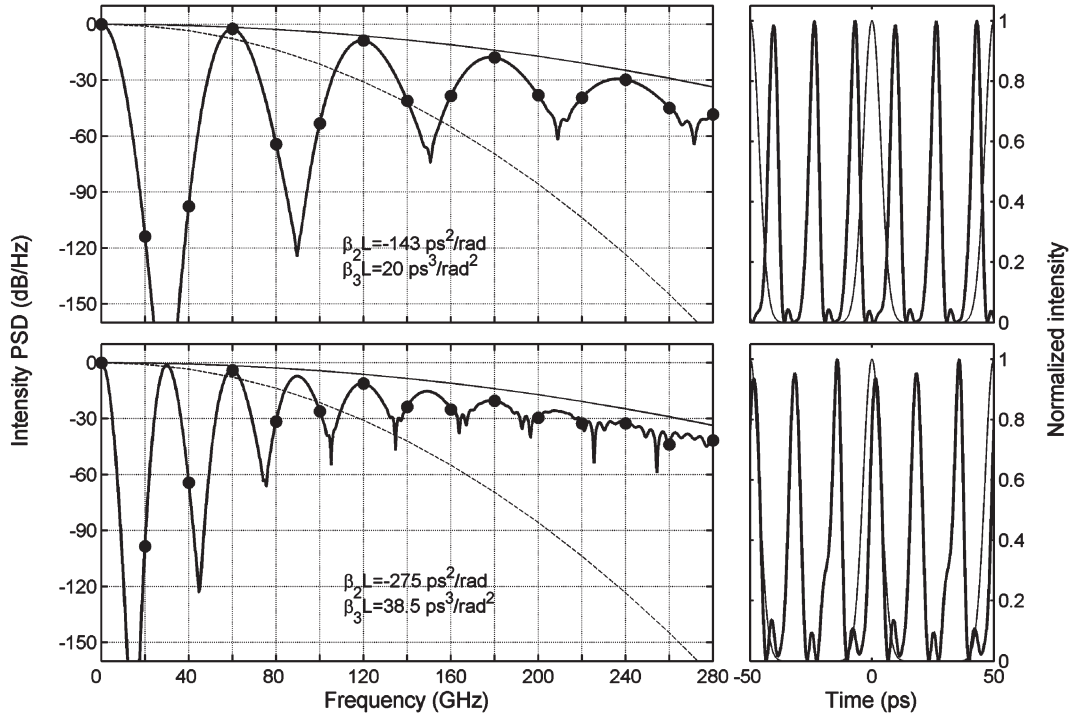


Fig. 5. Intensity PSD (left) and temporal intensity (right) of a 20-GHz train of 5-ps pulses after its propagation in a DSF of length $L = 285$ km (top) and 551 km (bottom), which correspond to the compressing Talbot condition with indexes $\gamma/\alpha = 1/3$ and $2/3$, respectively.

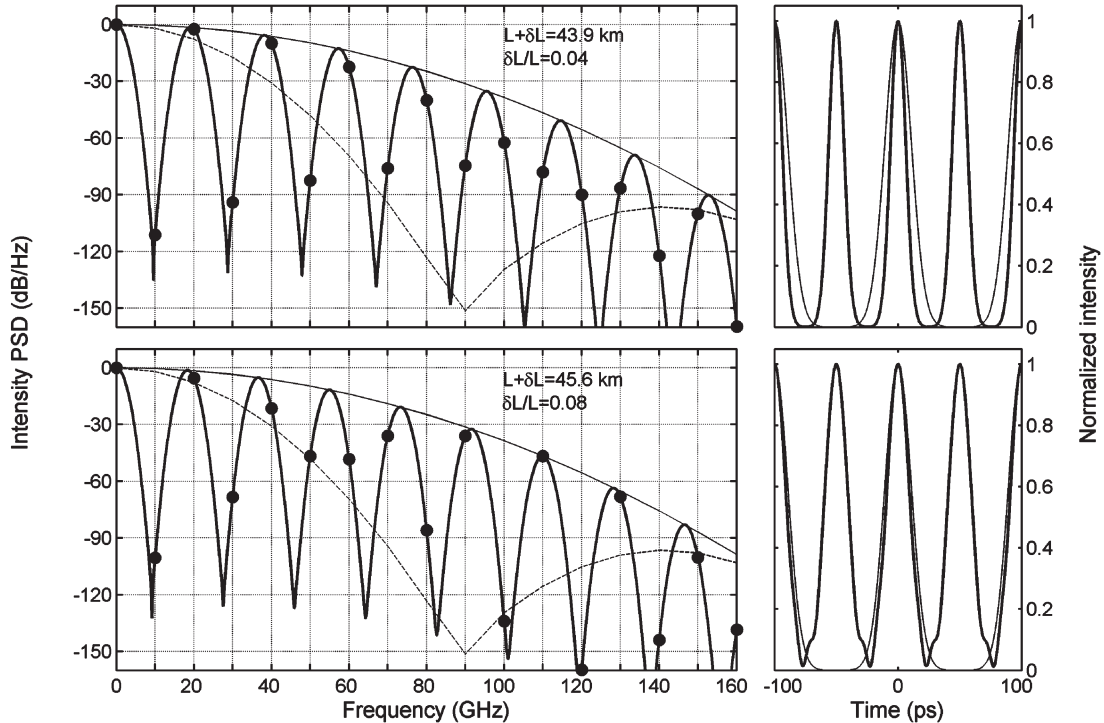


Fig. 6. Intensity PSD (left) and temporal intensity (right) of a 10-GHz train after its propagation in a standard SMF of length 43.9 km (top) and 45.6 km (bottom), which correspond to length deviations of the compressing Talbot condition with index $\gamma/\alpha = 1/2$. The relative length deviations are 4% and 8%, respectively.

IV. REJECTION PROPERTIES OF THE TALBOT FILTERS

As is well known, faithful reconstruction of the Talbot output train with increased repetition rate requires that pulses do not overlap. In the spectral domain, this fact is associated with the ability of the Talbot filter to reject residual RF harmonics. We

will briefly derive the nonoverlapping pulse condition directly from RF spectral analysis. This point of view is the basis of the tolerance analysis in the next section.

First, and because the overall bandwidth of the intensity spectrum is of the order of $3.72\sigma_\omega$ and the output harmonics are

multiples of $\alpha\Omega_0$, the following ratio determines the number of significant harmonics in the output train:

$$W = \frac{3.72\sigma_\omega}{\alpha\Omega_0} = \frac{2.23\sigma_{\omega\text{FWHM}}}{\alpha\Omega_0}. \quad (19)$$

In the last part of the formula, we have introduced the definition of W in terms of the spectral width measured as a full-width at half-maximum (FWHM). If the pulses are Gaussian, the relation of both spectral widths is $\sigma_{\omega\text{FWHM}} = 1.665\sigma_\omega$. Parameter W can also be interpreted as a normalized linewidth, because it is the overall spectral width of the train normalized by the fundamental output frequency. Because the temporal pulse duration goes as $1/\sigma_\omega$, W is also proportional to the number of pulses that can be contained in a period t_0/α of the output train.

Now, let us consider a general situation like those shown in Fig. 4 or 5. Let us assume that a given h th input harmonic is residual, i.e., it should not belong to the output train. Let us also consider that this harmonic will be filtered by a certain passband of index n and set the criterion that residual harmonics with power below -30 dB do not significantly alter the output signal. Thus, the following condition guarantees the filtering of residual harmonics:

$$|\omega_n - h\Omega_0| > \Delta_n\omega. \quad (20)$$

Using (14) and the definition of ω_n , this condition reads

$$\Omega_0|n\alpha - h\gamma| > \gamma\Delta_n\omega \quad (21)$$

with the most unfavorable situation being determined by the maximum of the right-hand side of (21) and by $|n\alpha - h\gamma| = 1$. Because α and γ are coprime integers, this equation can always be solved for n and h integers according to a corollary of Euclid's first theorem [28]. Therefore, all rejected harmonics lying in the significant portion of the spectrum ($\omega < 3.72\sigma_\omega$) carry an amount of power below -30 dB, if and only if $\Omega_0 > \gamma\Delta_{\omega\text{max}}$. This can be expressed as a lower bound K for W , which is written as

$$W > K = 2.20(1 + \varepsilon^2)^{\frac{1}{4}}. \quad (22)$$

This bound can be easily reinterpreted as the absence of pulse overlapping in the output train. For instance, if $W = 2.20$, second-order dispersion is negligible, and pulses are transform limited; hence, (22) is equivalent to the statement that 99% of the energy of the pulse is contained in the period t_0/α of the multiplied train.

V. STABILITY OF THE TALBOT FILTERS

By stability of the Talbot filters, we mean the ability of a dispersive line to create an intensity train with increased repetition-rate frequency under slight dispersion variations from compressing Talbot conditions. Compressing conditions will be considered as the ideal operation of the filter, because the harmonics of the output train lie at the center of the passbands. Standard Talbot conditions (13) can be considered as a length deviation $\delta L = C/\sigma_\omega^2 \cdot \beta_2$ from the compressing

condition (14). We will analyze the performance of the filters under the variations of the fiber length and the period of the input train.

First, timing variations can be reduced to length variations. Let us suppose that the frequency of the input train differs by a small quantity from the value used to determine the fiber length of the Talbot device. At first order, it can be interpreted as a deviation of the fiber length, because from (14), $\delta L/L = 2\delta\Omega_0/\Omega_0$, so that a relative change in the frequency of the train is equivalent to a double relative change in fiber length. Thus, Talbot filters are two times more sensitive to timing variations than to length variations.

Therefore, we focus on length variations δL . The result of this variation in the propagation of a train can be interpreted in two steps. The pulses of the input train are first dispersed individually under the accumulated dispersion $\beta_2\delta L$, and then, the filter acts ideally over the train of dispersed pulses. Therefore, the main spectral trace of a length variation of a compressing Talbot filter is the decrease of the RF bandwidth. However, length variations also affect the rejection properties of the dispersive filter.

These two features can be observed in the examples presented in Fig. 6, where the temporal signal and its intensity spectrum are depicted after the propagation along a standard SMF whose length has been enlarged by 4% (top) and 8% (bottom) from the compressing condition with index $\gamma/\alpha = 1/2$. Pulses have a width of 15 ps and chirp $C = 2$ rad. The second-order dispersion is negligible in both cases, i.e., $\varepsilon = 0.035$ (top) and $\varepsilon = 0.036$ (bottom). In the first example (top), the output signal can be entirely interpreted as a train of slightly dispersed pulses. In the second one, the additional broadening produces pulse-to-pulse interference and thus intensity fluctuations, observed as an increase in the power contained in the residual harmonics. Our tolerance analysis is precisely devoted to quantify the allowed changes in accumulated dispersion so that the interpretation of the output intensity as a train of nonoverlapping but slightly dispersed pulses is not missed.

From the spectral point of view, length or timing variations imply a deviation of the centers of the passbands $\delta\omega_n$ and a small change in their widths $\delta\Delta_n\omega$. These variations are, respectively, defined in the following equation [see (16) and (17) and the definition of ω_n]:

$$\frac{\delta\omega_n}{\omega_n} = \frac{\delta\Delta_n\omega}{\Delta_n\omega} = -\frac{\delta L}{L}. \quad (23)$$

First, let us consider the deviations in the spectral power of output harmonics, as shown in the first example in Fig. 6. The highest significant output harmonic ($\omega_n \cong 3.72\sigma_\omega$) suffers the most noticeable decrease in power due to pulse broadening. This harmonic has an index $n \cong \gamma W$, and its power does not fade more than 30 dB if

$$|\delta\omega_n| < \Delta_n\omega - |\delta\Delta_n\omega|. \quad (24)$$

This condition guarantees that the power of significant output harmonics follows a decreasing curve corresponding to a train

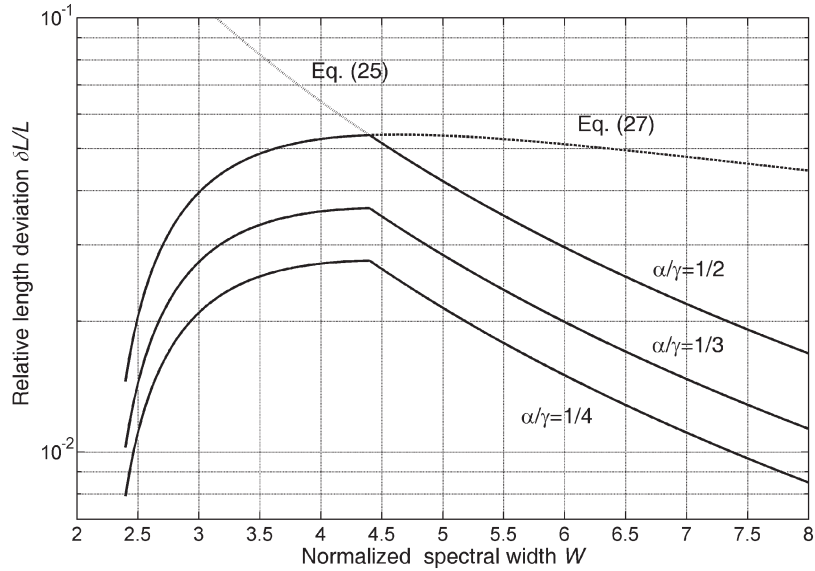


Fig. 7. Relative length deviation allowed by (25) and (27) with respect to the normalized spectral width W for different Talbot filters with negligible second-order dispersion.

of broader pulses. Using (14), (23), and (17), and the definition of W , (24) can be rewritten as

$$\frac{|\delta L|}{L} < \frac{K}{\alpha\gamma W^2 + K}. \quad (25)$$

This tolerance criterion essentially coincides with the bound (64) in [2], which was derived by considering the optical spectral phases induced by dispersion deviations.

On the other hand, it is necessary to assure that the power of all residual harmonics remains below -30 dB with respect to the carrier. This guarantees that, in the significant portion of the spectrum, the power of output harmonics is always larger than that of residual harmonics. This condition reads

$$|\omega_n - h\Omega_0| - |\delta\omega_n| > \Delta_n\omega + |\delta\Delta_n\omega|. \quad (26)$$

This equation is a generalization of (20). Following the same steps as in the previous section, we obtain

$$\frac{|\delta L|}{L} < \frac{W - K}{\alpha\gamma W^2 + K}. \quad (27)$$

Together, (25) and (27) determine the tolerance region where length variations induce an intensity train that can be interpreted, on one hand, as a train composed of slightly broadened pulses and, on the other, without significant intensity fluctuations.

Bounds (25) and (27) tend to approach zero in the limit of high spectral width [2], [5], [6]. Because parameter W controls the spectral purity of the output train, the quality of the output and the stability of the filter play opposite roles. To reach a compromise between quality and stability, we depict in Fig. 7 these bounds as a function of W for $\gamma/\alpha = 1/2$. The dotted

curve represents (25), whereas the dashed curve represents (27). The continuous curve represents the minimum of both curves. Below, the same minimum curves are depicted for different values of γ/α . Negligible second-order dispersion has been assumed ($K = 2.20$).

Bound (25) dominates at high W , so that the power of the output harmonics is very sensitive to the length deviations when the filter consists of narrow passbands or operates with narrow pulses with high spectral width. This is because narrow pulses may disperse considerably under small dispersion deviations. For small values of W , (27) dominates. In this regime, the efficiency of the filter is poor, because broad passbands or broad pulses allow residual harmonics to carry significant power. In other words, a certain amount of pulse interference is already present in the output in the absence of length variations as a nearly significant residual spectral power. Broader pulses do not disperse considerably under dispersion deviations, but a slight pulse interference augments the residual harmonic content. Therefore, the tolerance is dominated by the growth of residual harmonics.

Optimal tolerance is reached in the intersection point of both bounds, which is given by

$$W_{\text{opt}} = 2K. \quad (28)$$

This value verifies (22) and maximizes the stability of the Talbot line with a given index. Notice that the dependence on higher order dispersion is implicit in K . This is the proposed design criterion of the dispersive filter. Using the definition of W and assuming a negligible second-order dispersion, optimal tolerance condition (28) can be rephrased in terms of the spectral width of the input train. When it is measured as the FWHM, optimal conditions require that the FWHM is two times the repetition-rate frequency of the output train, i.e., $2\alpha\Omega_0$. From the temporal point of view and assuming transform-limited

pulses, this condition states that 99% of the energy of a pulse is contained in half a period of the multiplied train, i.e., $t_0/2\alpha$. The optimal value of tolerance is given by

$$\frac{|\delta L|}{L} < \frac{1}{4K\alpha\gamma + 1} \cong \frac{0.10}{\alpha\gamma(1 + \varepsilon^2)^{\frac{1}{4}}}. \quad (29)$$

Notice that it is inversely proportional to the product $\alpha\gamma$ and therefore to the complexity of the filter. When we consider the usual fractional Talbot filters of the series $\gamma/\alpha = 1/\alpha$, (29) states that the expected optimal tolerance in length is about 10% divided by the repetition-rate factor α . For instance, in the examples in Fig. 6, $W = 4.4$, and the tolerance in length given in (29) is 5%. Notice, finally, in Fig. 7 that optimal tolerance is located at the edge of a plateau. Nearly optimal tolerances can be obtained in its neighborhood.

VI. CONCLUSION

An analysis of the performance of Talbot dispersive lines, designed to increase passively the repetition-rate frequency of pulse trains, has been presented. It is based on the computation of the exact intensity PSD of a coherent train of pulses after its propagation in a dispersive medium with arbitrary first- and second-order dispersion and negligible attenuation. We have considered trains composed of linearly chirped Gaussian pulses. These analytical results permit the identification of the spectral components that represent the dispersion of individual pulses as well as the terms where the interference between pulses is enclosed.

Talbot dispersive lines can be interpreted as a multiple band-pass filter where each passband corresponds to the interference between pulses originally separated by a number of time slots. The filter essentially rejects the intensity harmonics of the input train that do not belong to the output. The rejection is exact only in semiinteger Talbot filters with a negligible higher order dispersion, because, in this case, the filter is adjusted to the dispersion of carrier suppression. The filter is not static but depends on the spectral width of the input train and the dispersive characteristics of the line. In particular, conditions that guarantee that the Talbot filter provides output intensity trains with negligible intensity fluctuations, even in the presence of higher order dispersion, have been derived. In these cases, however, the pulses may present distortion.

Finally, the stability under timing and length variations of the Talbot line has been analyzed. We have shown the properties of the two regimes of operation of Talbot filters, which are described by two bounds, namely (25) and (27). When the spectral width of the train is large, dispersion instabilities tend to broaden the pulses, and the filter's performance worsens by pulse-to-pulse interference. In contrast, when the spectral width is moderate, dispersion variations decrease the rejection ability of the filter. Optimal stability is reached when the spectral width of the input train, which is measured as FWHM, equals twice the repetition-rate frequency of the output train. The expected length tolerances are about 10% divided by the repetition-rate factor α .

REFERENCES

- [1] T. Jansson and J. Jansson, "Temporal self-imaging in single-mode fibers," *J. Opt. Soc. Amer.*, vol. 71, no. 11, pp. 1373–1376, Nov. 1981.
- [2] J. Azaña and M. A. Muriel, "Temporal self-imaging effects: Theory and application for multiplying pulse repetition rates," *IEEE J. Sel. Topics Quantum Electron.*, vol. 7, no. 4, pp. 728–744, Jul.–Sep. 2001.
- [3] P. A. Andrekson, "Linear propagation of optical picosecond pulse trains over oceanic distances," *Opt. Lett.*, vol. 18, no. 19, pp. 1621–1623, Oct. 1993.
- [4] I. Shake, H. Tahara, S. Kawanishi, and M. Saruwatari, "High-repetition-rate optical pulse generation by using chirped optical pulses," *Electron. Lett.*, vol. 34, no. 8, pp. 792–793, Apr. 1998.
- [5] S. Arahira, S. Kutsuzawa, Y. Matsui, D. Kunimatsu, and Y. Ogawa, "Generation of synchronized subterahertz optical pulse trains by repetition-frequency multiplication of subharmonic synchronous mode-locked semiconductor laser diode using fiber dispersion," *IEEE Photon. Technol. Lett.*, vol. 10, no. 2, pp. 209–211, Feb. 1998.
- [6] —, "Repetition-frequency multiplication of mode-locked pulses using fiber dispersion," *J. Lightw. Technol.*, vol. 16, no. 3, pp. 405–410, Mar. 1998.
- [7] J. Fatome, S. Pitois, and G. Millot, "Influence of third-order dispersion on the temporal Talbot effect," *Opt. Commun.*, vol. 234, no. 1–6, pp. 29–34, Apr. 2004.
- [8] S. Longhi, M. Marano, P. Laporta, O. Svelto, M. Belmonte, B. Agogliati, L. Arcangeli, V. Pruneri, M. N. Zervas, and M. Ibsen, "40-GHz pulse-train generation at 1.5 μm with a chirped fiber grating as a frequency multiplier," *Opt. Lett.*, vol. 25, no. 19, pp. 1481–1483, Oct. 2000.
- [9] N. K. Berger, B. Levit, A. Bekker, and B. Fischer, "Compression of periodic optical pulses using temporal fractional Talbot effect," *IEEE Photon. Technol. Lett.*, vol. 16, no. 8, pp. 1855–1857, Aug. 2004.
- [10] S. Longhi, M. Marano, P. Laporta, and V. Pruneri, "Multiplication and reshaping of high-repetition-rate optical pulse trains using highly dispersive fiber Bragg gratings," *IEEE Photon. Technol. Lett.*, vol. 12, no. 11, pp. 1498–1500, Nov. 2000.
- [11] J. H. Lee, Y. M. Chang, Y.-G. Han, S. H. Kim, and S. B. Lee, "2 ~ 5 times tunable repetition-rate multiplication of a 10 GHz pulse source using a linearly tunable, chirped fiber Bragg grating," *Opt. Express*, vol. 12, no. 17, pp. 3900–3905, Aug. 2004.
- [12] J. A. Bogler, P. Hu, J. T. Mok, J. L. Blows, and B. J. Eggleton, "Talbot self-imaging and cross-phase modulation for generation of tunable high repetition rate pulse trains," *Opt. Commun.*, vol. 249, no. 4–6, pp. 431–439, May 2005.
- [13] C. J. S. de Matos and J. R. Taylor, "Tunable repetition-rate multiplication of a 10 GHz pulse train using linear and nonlinear fiber propagation," *Appl. Phys. Lett.*, vol. 83, no. 26, pp. 5356–5358, Dec. 2003.
- [14] D. A. Chestnut, C. J. S. de Matos, and J. R. Taylor, "4 \times repetition-rate multiplication and Raman compression of pulses in the same optical fiber," *Opt. Lett.*, vol. 27, no. 14, pp. 1262–1264, Jul. 2002.
- [15] S. Atkins and B. Fischer, "All-optical pulse rate multiplication using fractional Talbot effect and filed-to-intensity conversion with cross-gain modulation," *IEEE Photon. Technol. Lett.*, vol. 15, no. 1, pp. 132–134, Jan. 2003.
- [16] J. Azaña, N. K. Berger, B. Levit, V. Smulakovsky, and B. Fischer, "Frequency shifting of microwave signals by use of a general temporal self-imaging (Talbot) effect in optical fibers," *Opt. Lett.*, vol. 29, no. 24, pp. 2849–2851, Dec. 2005.
- [17] J. T. Mok and B. J. Eggleton, "Impact of group delay ripple on repetition-rate multiplication through Talbot self-imaging effect," *Opt. Commun.*, vol. 232, no. 1–6, pp. 167–178, Mar. 2004.
- [18] K. Jürgensen, "Transmission of Gaussian pulses through monomode dielectric optical waveguides," *Appl. Opt.*, vol. 16, no. 1, pp. 22–23, Jan. 1977.
- [19] —, "Gaussian pulse transmission through monomode fibers, accounting for source linewidth," *Appl. Opt.*, vol. 17, no. 15, pp. 2412–2415, Aug. 1978.
- [20] B. E. A. Saleh and M. I. Irshid, "Transmission of pulse sequences through monomode fibers," *Appl. Opt.*, vol. 21, no. 23, pp. 4219–4222, Dec. 1982.
- [21] —, "Coherence and intersymbol interference in digital fiber optics communication systems," *IEEE J. Quantum Electron.*, vol. QE-18, no. 6, pp. 944–951, Jun. 1982.
- [22] M. A. Muriel and J. Capmany, "Optical pulse sequence transmission through monomode fibres under second and third-order dispersion," *Electron. Lett.*, vol. 24, no. 19, pp. 1252–1253, Sep. 1988.
- [23] J. Capmany and M. A. Muriel, "Optical pulse sequence transmission through single-mode fibers: Interference signal analysis," *J. Lightw. Technol.*, vol. 9, no. 1, pp. 27–36, Jan. 1991.

- [24] J. Azaña, "Pulse repetition rate multiplication using phase-only filtering," *Electron. Lett.*, vol. 40, no. 7, pp. 449–451, Apr. 2004.
- [25] G. P. Agrawal, *Nonlinear Fiber Optics*, 3rd ed. Boston, MA: Academic, 2001.
- [26] C. Dorrer and D. N. Maywar, "RF spectrum analysis of optical signals using nonlinear optics," *J. Lightw. Technol.*, vol. 22, no. 1, pp. 266–274, Jan. 2004.
- [27] H. Schmuck, "Comparison of optical millimeter-wave systems with regard to chromatic dispersion," *Electron. Lett.*, vol. 31, no. 21, pp. 1848–1849, Oct. 1995.
- [28] G. H. Hardy and E. M. Wright, *An Introduction to the Theory of Numbers*, 5th ed. Oxford, U.K.: Clarendon, 1995, ch. 2, p. 21. th. 26.



Carlos R. Fernández-Pousa (M'05) was born in Ourense, Spain, in 1970. He received the B.S., M.S., and Ph.D. degrees in physics from the University of Santiago de Compostela, Santiago de Compostela, Spain, in 1993, 1994, and 1998, respectively, with a thesis on the classical and quantum theory of solitons.

In 1997, he joined the Universidad Miguel Hernandez, Elche, Spain, where he is an Associate Professor. His research interests include diffractive, polarization, and GRIN optics, coherence, propagation in guided media, laser physics, and frequency conversion.

Dr. Fernández-Pousa is a member of SEDO and OSA.



Carlos Gómez-Reino was born in Pontevedra, Spain, in 1946. He received the B.S., M.S., and Ph.D. degrees in physics from the Complutense University of Madrid (UCM), Madrid, Spain, in 1968, 1970, and 1975, respectively.

From 1969 to 1979, he was an Assistant Professor of optics at the UCM. Since 1980, he has been a Professor of optics at the Faculty of Physics and Optics and Optometry School, University of Santiago de Compostela, Santiago de Compostela, Spain. He has signed more than 150 papers published in peer-

reviewed scientific journals, mainly on zone plates and integrated and GRIN optics. He is a coauthor of *GRIN Optics: Fundamentals and Applications* (Berlin, Germany: Springer, 2002).

Dr. Gómez-Reino is a member of the RSEF, SEDO, OSA, SPIE, AAAS, and NYAS and is a Fellow of the Optical Society of America.



Laura Chantada was born in A Coruña, Spain, in 1979. She received the B.S. and M.S. degrees in physics from the University of Santiago de Compostela, Santiago de Compostela, Spain, in 2001 and 2003, respectively. She is currently working toward the Ph.D. degree in the temporal Talbot effect at the University of Santiago de Compostela.

Her research interests include space–time duality, pulse propagation in dispersive media, optical coherence, and nanostructures.